Influence of Ti(C,N) precipitates on austenite growth of micro-alloyed steel during continuous casting

Liu Yang [1, 2], *Yang Li [1], Zheng-liang Xue [1], and Chang-gui Cheng [1]

1. The State Key Laboratory of Refractories and Metallurgy, Wuhan University of Science and Technology, Wuhan 430081, China

2. Steelmaking Plant of WISCO, Wuhan 430083, China

Abstract: Austenite grain size is an important influence factor for ductility of steel at high temperatures during continuous casting. Thermodynamic and kinetics calculations were performed to analyze the characteristics of Ti(C,N) precipitates formed during the continuous casting of micro-alloyed steel. Based on Andersen-Grong equation, a coupling model of second phase precipitation and austenite grain growth has been established, and the influence of second precipitates on austenite grain growth under different cooling rates is discussed. Calculations show that the final sizes of austenite grains are 2.155, 1.244, 0.965, 0.847 and 0.686 mm, respectively, under the cooling rate of 1, 3, 5, 7, and 10 ℃·s^{-1}, when ignoring the pinning effect of precipitation on austenite growth. Whereas, if taking the pinning effect into consideration, the grain growth remains stable from 1,350 ℃, the calculated final sizes of austenite grains are 1.46, 1.02, 0.80, 0.67 and 0.57 mm, respectively. The sizes of final Ti(C,N) precipitates are 137, 79, 61, 51 and 43 nm, respectively, with the increase of cooling rate from 1 to 10 ℃·s^{-1}. Model validation shows that the austenite size under different cooling rates coincided with the calculation results. Finally, the corresponding measures to strengthen cooling intensity at elevated temperature are proposed to improve the ductility and transverse crack of slab.

Key words: micro-alloyed steel; Ti(C,N) precipitation; austenite grain; pinning effect

CLC numbers: TG249.7/142.25/TP391.99 **Document code:** A **Article ID:** 1672-6421(2017)05-421-08

According to thermal mechanical control process and relaxation-precipitation controlling phase transformation technique during hot rolling process, the microstructure of steel can be refined by the addition of Ti-Nb microalloys [1, 2]. A significant improvement in strength, toughness and weldability of steel can be obtained by Ti(C,N) precipitation. However, the hot ductility of micro-alloyed steels remains very poor during continuous casting, which leads to the formation of transverse cracks during the straightening process [3, 4]. The influence factors of hot ductility in the third brittle zone include the size of austenite grain, carbonitride precipitation and pro-eutectoid ferrite film [5, 6].

Research concerning the impact of Ti(C,N) precipitation on the growth of austenite mainly focuses on the hot rolling process at current stage [7-11]. However, there has been few investigations of austenite growth during continuous casting, which affects the ductility of steel directly. The formation of coarse austenite grain during soft cooling of strand surface below oscillation marks in slabs usually deteriorates ductility and causes transverse cracks in the straightening process. Therefore, the prediction of austenite grain size in micro-alloyed steels is very important.

The main challenge in the size prediction of austenite grains is the computational complexity of $f(t)/r(t)$ in the Andersen-Grong equation, where f is the volume fraction and r the radius of the precipitates, which is related to the nucleation and growth of precipitates at each state including temperature and time. By implementing some simulation models, Miettinen et al[12] fitted the results of Yasumoto's experimental data[13] using Equation (1). For the steel grade with carbon equivalent of 0.17%, the maximum grain size was found at the highest temperature for totally austenitic structure. Bernhard et al.[14] analyzed the influence of pinning

***Yang Li**

Female, born in 1988, Ph.D. Associate Professor. Research interests: microstructure transformation and quality control in continuous casting.

E-mail: liyang@wust.edu.cn

Received: 2017-7-11; Accepted: 2017-09-03

precipitates of AlN on austenite growth, and the final austenite grain size was 0.53 mm when w[N]=0.0080% and q_p=2.52×10^3 m^{-1}. Based on the Andersen-Grong equation, a model coupling austenite growth with precipitates growth was established in this work to study the impact of precipitation on the austenite growth under different cooling rates.

$$\overline{D} = 21 \cdot T_\gamma \ -3152 \cdot \frac{e^{V_C}}{1-e^{V_C}} - 25088 \qquad (1)$$

In Equation (1), T_γ denotes the highest temperature of a totally austenitic structure, ℃; V_c is the cooling rate of solidification, ℃·s^{-1}; and $\overline{D}$ is the final austenite grain size, μm.

1 Thermodynamics and kinetics of Ti(C, N) precipitation

1.1 Thermodynamics

In order to describe the changing characteristics of carbonitride precipitates of steel at different temperatures, the solubility product is applied:

$$\lg K = \lg\{[\mathrm{M}]\cdot[\mathrm{X}]\} = A - B/T \qquad (2)$$

where, T represents absolute temperature, K, [M] and [X] are weight fractions of dissolved metal element M (Nb, Ti and V et al) and non-metal element X(C,N), respectively. A, B are the regression coefficients in solubility product lg$K$. The equilibrium solid solubility product of Ti(C,N) precipitates with temperature is shown in Table 1.

Table 1: Solubility product of Ti(C,N) precipitates in different phases [15]

	Solid Solubility (lg$K$)		
	Molten steel	Austenite	Ferrite
TiN	5.9–16580/T	0.32–8000/T	6.4–18420/T
TiC	5.317–9393/T	2.75–7000/T	4.45–10230/T

The change of equilibrium solid solubility of Ti(C,N) precipitates in different phases at different temperatures is shown in Fig. 1. Because of a lower equilibrium solubility compared to TiC, TiN has good stability in molten steel, austenite and ferrite. The equilibrium solubility product of TiN is about 1×10^{-3} at elevated temperature, so it can be speculated that TiN could precipitate in molten steel [16]. Additionally, since the equilibrium solubility product of TiN is as low as 10^{-4}–10^{-5} at austenitic temperature, controlling TiN precipitation is widely used to refine austenite grain.

Table 2 lists the actual composition of experimental grade steel. Equation (3) is used to describe the simultaneous equation of TiN and TiC solubility product, and the ideal stoichiometric of Ti, C and N in Ti(C_xN_{1-x}) precipitates, in which x is partition

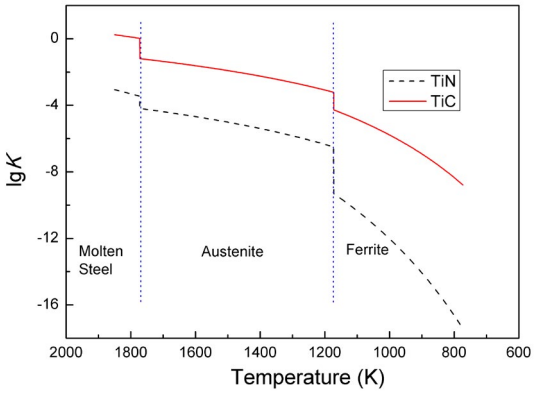

Fig. 1: Equilibrium solid solubility of TiC, TiN precipitates in different phases

Table 2: Actual composition of experimental grade steel (wt.%)

C	Si	Mn	Als	Mo	Cr	Ti	Nb	N
0.111	0.235	1.473	0.0415	0.100	0.332	0.015	0.0318	0.0030

coefficient [17]. Figure 2 shows the relationship between equilibrium concentration as well as partition coefficient x of Ti(C_xN_{1-x}) precipitates and temperature obtained through Equation (3). As temperature decreases, the equilibrium contents of Ti and N in austenite gradually decrease, while x gradually increases. The partition coefficient x is only about 0.04 when the temperature is between 1,350 ℃ and 1,440 ℃, which means the Ti(C_xN_{1-x}) precipitates at high temperature is close to pure TiN.

$$\begin{cases} \lg\dfrac{[\mathrm{M}]\cdot[\mathrm{C}]}{x} = A_1 - B_1/T \\ \lg\dfrac{[\mathrm{M}]\cdot[\mathrm{N}]}{1-x} = A_2 - B_2/T \\ \dfrac{\mathrm{M}-[\mathrm{M}]}{\mathrm{C}-[\mathrm{C}]} = \dfrac{\mathrm{A_M}}{x\cdot\mathrm{A_C}} \\ \dfrac{\mathrm{M}-[\mathrm{M}]}{\mathrm{N}-[\mathrm{N}]} = \dfrac{\mathrm{A_M}}{(1-x)\cdot\mathrm{A_N}} \end{cases} \qquad (3)$$

where, M, C, N are weight fractions of dissolved element in molten steel, and x is the partition coefficient in Ti(C_xN_{1-x}) precipitates.

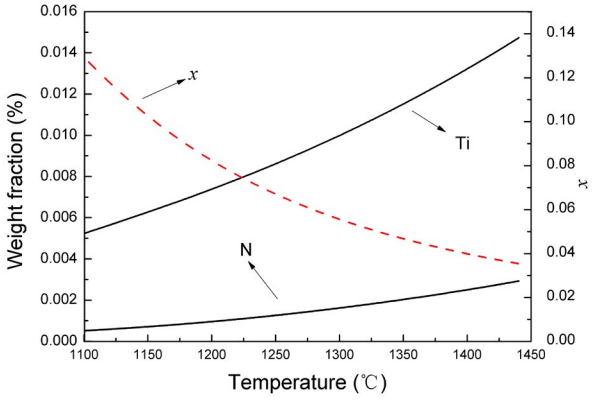

Fig. 2: Equilibrium concentration of Ti and N and partition coefficient x in precipitates

1.2 Kinetics

The extent of precipitation, and the relationship between precipitation temperature and time are described by the kinetics of Ti(C,N) precipitation, and is mainly dependent on the nucleation rate and growth rate of precipitates. Based on the kinetics calculation results, the PTT (Precipitation Temperature Time) curve of Ti(C,N) is plotted in Fig. 3, and it has the typical "C" characteristics. The nucleation rate of Ti(C,N) is very low at higher temperatures with a large component diffusion, but is higher at lower temperatures with less component diffusion. Compared to homogeneous nucleation, austenite grain boundary nucleation with a critical nucleation work of 10^{-19} J·mol^{-1} at high temperature calculated by linear interpolation is preferred for the nucleation location.

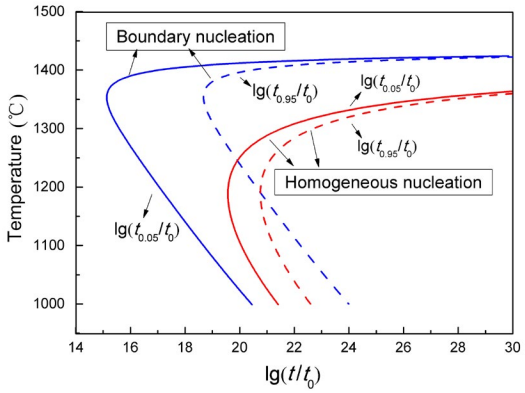

Fig. 3: PTT curve of Ti(C,N) precipitation

($lg(t_{0.05}/t_0)$ as the starting time of precipitation; $lg(t_{0.95}/t_0)$ as the ending time of precipitation)

2 Coupling model of second phase precipitation and austenite grain growth

Based on the Andersen-Grong equation, a coupling model of second phase precipitation and austenite grain growth has been established. The hypotheses for the model include:

(a) Precipitates are stoichiometric Ti(C_xN_{1-x}), and thermodynamic parameters are calculated by the linear interpolation method based on TiC and TiN;

(b) Precipitates are assumed to be spherical for easy calculation;

(c) The local temperature is a simple time-dependent function under the certain cooling condition;

(d) The diffusion coefficient of Ti is very small compared to that of C and N;

(e) Due to the same temperature range between the starting time of precipitation and T_γ, the precipitate and austenite growth perform simultaneously.

2.1 Austenite growth

Based on Andersen-Grong's differential equations [18], the change of average austenite grain size ($\overline{D}$) with time t and temperature T in the presence of pinning precipitates is given by Equation (4):

$$\frac{\mathrm{d}\overline{D}}{\mathrm{d}t} = M_0^* \cdot \exp\left(-\frac{Q_{app}}{R \cdot T}\right) \cdot \left(\frac{1}{\overline{D}} - \frac{q_p}{k}\right)^{\left(\frac{1}{n}-1\right)} \quad (4)$$

In this equation, M_0^* denotes a kinetic constant that describes the grain boundary mobility, assumed as 4×10^{-3} m^2·s^{-1} [14], and R is the gas constant (8.3145 J·mol^{-1}·K^{-1}). k/q_p represents the maximum grain diameter under normal conditions, k denotes Zener limit coefficient, equal to 4/3 in this model. Exponent n is at most equal to 0.5 according to an analysis of grain growth data [19]. Q_{app} is the apparent activation energy for grain growth, J·mol^{-1}, as shown in Equation (5) [20]. c_p denotes equivalent carbon content, weight percent.

$$Q_{app} = 167686 + 40.562 \cdot c_p \quad (5)$$

Using the Runge-Kutta method, Equation (4) can be simplified to Equation (6). Impacted by precipitation at the boundary, the driving force will be counteracted by the pinning force. When the initial austenite grain is infinitely small, the driving force will be infinite, which is not allowed in the mathematical model. The initial temperature of austenite transformation is set to 1,440 ℃ in the model [5], and the initial austenite grain size is set to 100 μm, which is in the range of primary dendrite arm spacing.

$$\overline{D}(t+\Delta t) = \overline{D}(t) + M_0^* \cdot \exp\left(-\frac{2Q_{app}}{R\cdot(T_i+T_{i+1})}\right) \cdot \left(\frac{1}{\overline{D}(t)} - \frac{q_p}{k}\right) \cdot \Delta t \quad (6)$$

2.2 Ti(C,N) precipitation

The term k/q_p in Equation (4) represents the retardation of grain growth by particles. According to Equation (7), q_p is the fraction $f(t)/r(t)$ for all classes of precipitates [14]. As the temperature decreases, Ti(C_xN_{1-x}) precipitates with different nucleation rates and growth rates, and Equation (7) translates into Equation (8). q_p is calculated by Equation (8) and related to the summation of the product of nucleation $N(t, \tau)$ and $r(t, \tau)^2$ at different nucleation times τ per volume of the system.

$$q_p(t) = \frac{f(t)}{r(t)} \quad (7)$$

$$q_p(t) = \frac{4\pi}{3}\sum_{\tau=0}^{\tau=t}[r(t,\tau)^2 \cdot N(t,\tau)] \quad (8)$$

where, $f(t)$ is the volume fraction and $r(t)$ is the radius of the precipitates, *m*. $N(t, \tau)$ and $r(t, \tau)^2$ represents the nucleation and radius of particles size squared at certain nucleation time τ.

The nucleation rate per volume $\frac{\mathrm{d}N(t)}{\mathrm{d}t}$ is calculated by Equation (9) [14]:

$$\frac{\mathrm{d}N(t)}{\mathrm{d}t} = N_0 D_{Ti}(T) \cdot [\mathrm{Ti}]_\infty e^{\frac{\Delta G_g^*}{k_B T}} \quad (9)$$

where, N_0 represents a factor that is proportional to the density of nucleation sites, and assumed as 3.25×10^{25} m^{-5} in this model. The Boltzmann constant k_B is 1.38×10^{-23} $J\cdot K^{-1}$. $D_{Ti}(T)$ is the effective diffusion coefficient of Ti in austenite, $m^2\cdot s^{-1}$.

The free energy (J) of critical nucleation is given by Equation (10):

$$\Delta G^* = \frac{16\pi\sigma^3}{\Delta G_V} \tag{10}$$

where, σ is interfacial tension between the precipitates and steel, $J\cdot m^{-2}$. ΔG_V is free energy of nucleation per unit volume, $J\cdot m^{-3}$.

When the second phase precipitates at the grain boundary, the critical nucleation work ΔG_g^*(J) will be reduced to Equation (11):

$$\Delta G_g^* = A_0 \times \Delta G^* \tag{11}$$

where, A_0 is related to the contact angle between generated precipitates and base phase. $A_0 = \frac{1}{2}(2-3\cos\theta+\cos^3\theta)$, and cosθ = 0.835414 [21].

With the diffusion coefficient constant $D_{0,Ti}$ being 1.5×10^{-5} $m^2\cdot s^{-1}$, and activation energy of diffusion $Q_{D,Ti}$ being 251,000 $J\cdot mol^{-1}$, the effective diffusion coefficient ($m^2\cdot s^{-1}$) of Ti in austenite is given by Equation (12) [17]:

$$D_{Ti}(T) = D_{0,Ti}\cdot e^{-\frac{Q_{D,Ti}}{R\cdot T}} \tag{12}$$

Assuming the growth of Ti(C_xN_{1-x}) precipitates is controlled by Ti diffusion, according to the Zener's growth equation, the growth rate v ($m\cdot s^{-1}$) of Ti(C_xN_{1-x}) precipitates can be described by Equation (13) [22]:

$$v = \frac{dr}{dt} = \frac{D_{Ti}(T)}{r}\frac{X_0 - X_e}{X_p - X_e} \tag{13}$$

where, X_0 and X_e denote the Ti concentration in the matrix and austenite grain boundary, X_p represents the Ti concentration in the Ti(C_xN_{1-x}) phase with value of 1 [23].

The conversion relation between weight concentration and molar concentration is shown in Equation (14).

$$c_B = \frac{w_B\rho_{Fe}}{100A_B} \tag{14}$$

where, w_B is weight concentration in steel, c_B is molar concentration in steel, and ρ_{Fe} is density of austenite.

By solving differential Equation (13), Equation (15) can be acquired by mass concentration.

$$r(t+\Delta t)^2 = r(t)^2 + 2D_{Ti}\frac{w_0 - w_e}{\frac{100A_{Ti}}{\rho_{Fe}} - w_e}\cdot\Delta t \tag{15}$$

2.3 Model calculation

The algorithm of the coupling model is expatiated in Table 3. Figure 4 describes the process of obtaining $q_p(t)$, which is the most complicated calculation in the model.

Table 3: Algorithm of austenite growth

Steps	Algorithm	Notes
1:	Set Diameter =1×10^{-4} m, Q_{app}=173238.9 J/m^2, t=T=T_γ=1440 ℃;	
2:	Set Δt = 1℃/V_C, $r(t)^2$ = initial value;	
3:	While t>1200 Do	
4:	Set i = 0, q_p = 0;	Initialization
5:	While T>t Do	
6:	Compute x, [Ti], [N]	Iterative computations
7:	Compute A, B, ΔG_m, V_m, σ;	Linear interpolation calculation
8:	Compute ΔG_g^*, $dN(t)/dt\cdot\Delta t$;	See Equation (9), Equation (10)
9:	Compute $r(t)^2$;	See Equation (15)
10:	Compute q_p;	See Equation (8)
11:	Set i = i+1, T =T–1;	
12:	End While	
13:	Compute Diameter;	See Equation (6)
14:	Set t = t–1	
15:	End While	

Note: V_m is the molar volume of the precipitates, $m^3\cdot mol^{-1}$.

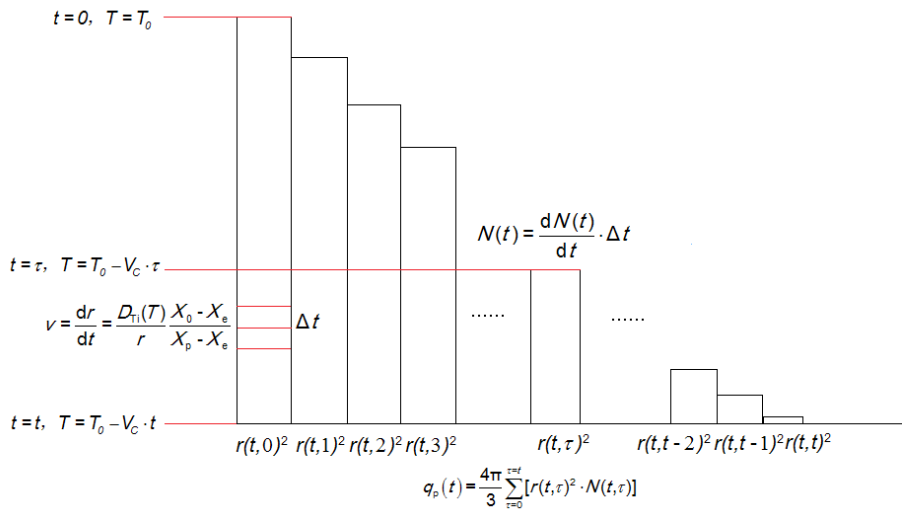

Fig. 4: Process of calculating $q_p(t)$ in model

Notes: Taking V_C into account, the parameter τ in the model is used as one of array index in each temperature gradient based on hypotheses (c).

2.4 Model results

When ignoring the pinning effect of precipitates on austenite, the Andersen-Grong equation is solved as in the following Equation (16). The results show that the duration (Δt=1 ℃/V_C) of each temperature gradient for austenite growth decreases with an increase in the cooling rate, which leads to a slowdown of austenite growth. In addition, the growth of austenite is substantially faster at higher temperature, because of the larger $\frac{1}{\bar{D}(t)}$ in the austenite growth coefficient $M_0^* \cdot \exp\left(-\frac{2Q_{app}}{R\cdot(T_i+T_{i+1})}\right)\cdot\left(\frac{1}{\bar{D}(t)}\right)$. Finally, the sizes of austenite grains are 2.155, 1.244, 0.965, 0.847 and 0.686 mm, respectively, when the cooling rate is set to 1, 3, 5, 7 and 10 ℃·s^{-1}, as shown in Fig. 5.

$$\bar{D}(t+\Delta t) = \bar{D}(t) + M_0^* \cdot \exp\left(-\frac{2Q_{app}}{R\cdot(T_i+T_{i+1})}\right)\cdot\frac{\Delta t}{\bar{D}(t)} \quad (16)$$

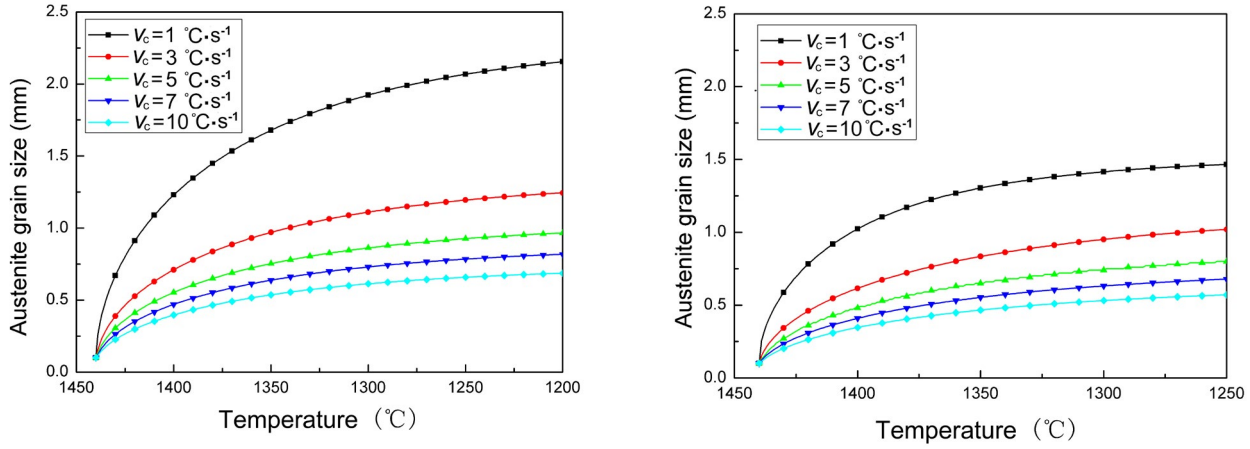

Fig. 5: Effect of cooling rate on austenite growth (left: non-pinning effect model; right: pinning effect model)

When considering the pinning effect of precipitates on austenite, the austenite growth coefficient will be altered to $M_0^* \cdot \exp\left(-\frac{2Q_{app}}{R\cdot(T_i+T_{i+1})}\right)\cdot\left(\frac{1}{\bar{D}(t)}-\frac{q_p}{k}\right)$, and the driving force for austenite growth will decrease as the temperature decreases. The comparison between the non-pinning and pinning effects on austenite is listed in Table 4. In the pinning effect model, grain growth becomes stable from 1,350 ℃, which results in a final austenite grain size of only 1.46, 1.02, 0.80, 0.67 and 0.57 mm.

Table 4: Final austenite grain size with non-pinning and pinning effects on austenite (mm)

	Cooling rate (℃·s^{-1})				
	1	3	5	7	10
Non-pinning effect	2.15	1.24	0.96	0.84	0.68
Pinning effect	1.46	1.02	0.80	0.67	0.57

The change of average sizes of Ti(C_xN_{1-x}) precipitates with temperature under different cooling rates is illustrated in Fig. 6. It can be seen that the Ti(C_xN_{1-x}) precipitates are smaller at a higher cooling rate. At high temperatures ($1{,}350℃ \leq T \leq T_\gamma$), the Ti($C_xN_{1-x}$) precipitates grow rapidly with a higher diffusion coefficient of Ti and solubility element (Ti, N) around the austenite grain boundaries, and then gradually reach stability from 1,350 ℃. The final sizes are 137, 79, 61, 51 and 43 nm, respectively, with an increase in the cooling rate as described in Fig. 7.

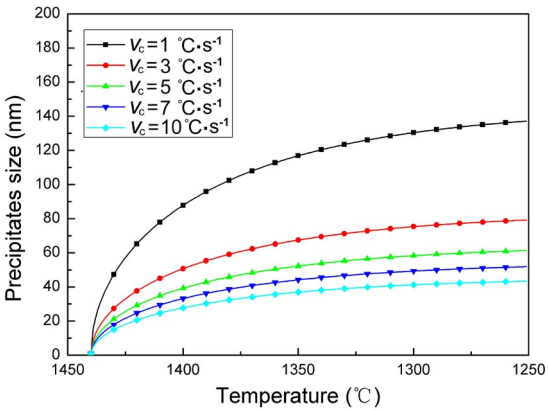

Fig. 6: Average sizes of Ti(C_xN_{1-x}) precipitates with temperature under different cooling rates (nm)

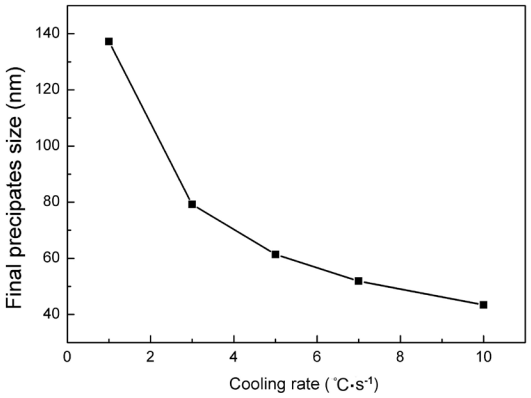

Fig. 7: Final sizes of Ti(C_x,N_{1-x}) precipitates under different cooling rates

3 Model validation

The tensile specimens were taken from 1/4 section of casting slab in the plant, and processed into Φ6 mm×120 mm along the casting direction with standard thread M6×1.0-6g at both ends of specimens. With the aid of a Gleeble-3500 thermal simulator, the influence of Ti(C,N) precipitates on austenite growth was implemented under different cooling rates. Figure 8 shows the temperature schedules in the thermal tensile test. Firstly, the surface temperature of the specimen was heated to 1,400 ℃, measured by "R" thermocouple, and the core temperature is assumed to be about 1,500 ℃ through a series of tests. Then the specimen was held 20 seconds to ensure complete dissolution of the Ti(C,N) precipitates and δ-ferrite, and then cooled to 1,200 ℃ with the cooling rates of 10, 7, 5, 3, and 1 ℃·s^{-1}, respectively. Finally, the specimens were quenched by a high speed compressed air flow to freeze the steel structure at high temperature. In order to observe the austenite boundaries, the fracture samples were polished and etched with saturated picric acid [24] and a small amount of shampoo in the 80 ℃ water bath for 8 minutes.

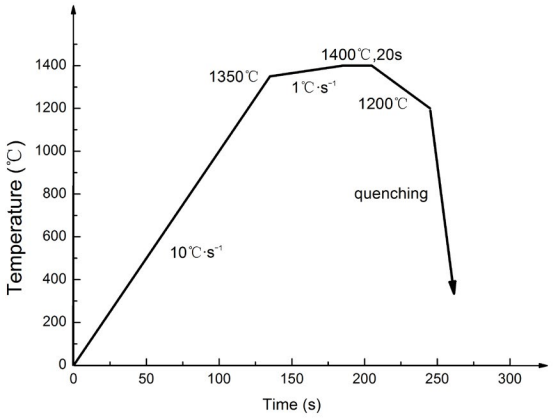

Fig. 8: Temperature schedules in thermal tensile test

Figure 9 is the typical micrograph of the fracture samples etched with saturated picric acid. The austenite boundaries can be clearly distinguished. It can be observed that along the former austenite grain boundaries several lath martensites are formed in an austenite grain. The final austenite sizes are 300 μm to 2,000 μm under different cooling conditions. Owing to the coarse austenite grains of continuous casting slabs, the etched micrographs with manually traced austenite grain boundaries are created by mixing micrographs, as shown in Fig. 10. According to the measuring method of the average grain size of metal in GB6394-2002, the austenite grain sizes under different the cooling rates of 1, 3, 5, 7 ,10 ℃·s^{-1} are obtained and shown in the Table 5, which are 1.41, 1.08, 0.78, 0.61, and 0.48 mm, respectively.

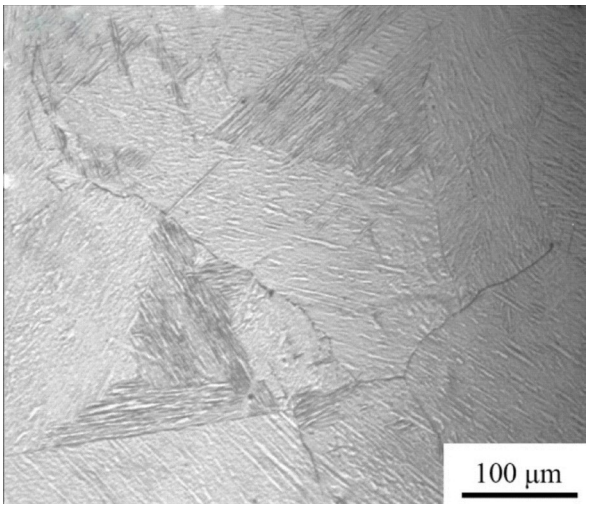

Fig. 9: Martensite and austenite grain boundaries in etched micrograph

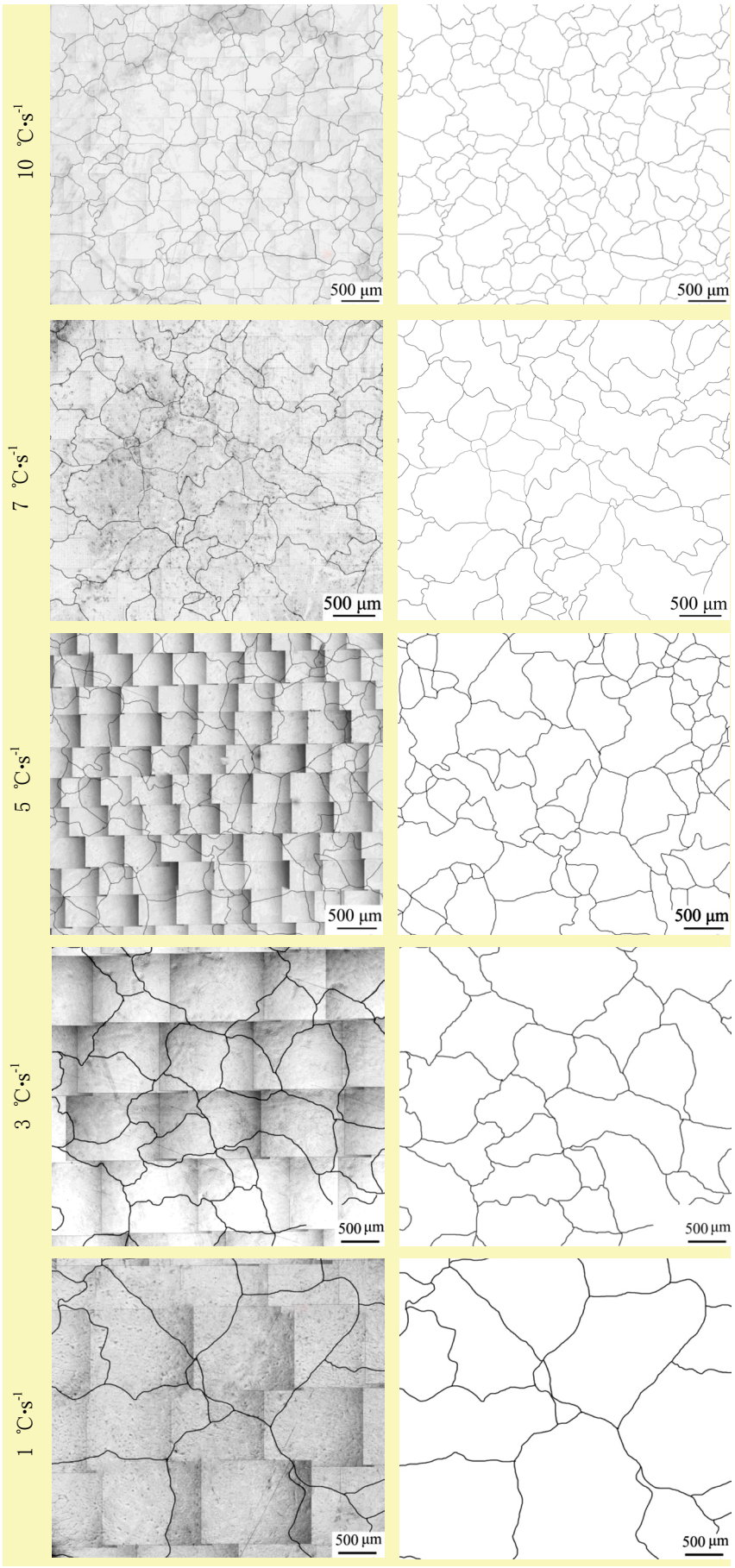

Fig. 10: Etched micrograph with manually traced austenite grain boundaries

(Left: micrograph and traced austenite grain boundaries; Right: traced austenite grain boundaries.)

Figure 11 demonstrates the comparison of predicted sizes to measured sizes of austenite grains under different cooling rates. It shows that the austenite size is finer under higher cooling rate, and the computational model result is consistent with the experiment data. The nucleation and growth of the austenitic grains are both an atomic diffusion process, and mainly related to the grain boundary migration rate, which is mainly influenced by the velocity of the atomic diffusion near the grain boundary. Meanwhile, according to the Andersen-Grong equation, the duration for austenite growth Δt=1 ℃/V_C is shortened, and the growth coefficient

$$M_0^* \cdot \exp\left(-\frac{2Q_{app}}{R\cdot(T_i+T_{i+1})}\right)\cdot\left(\frac{1}{\bar{D}(t)}-\frac{q_p}{k}\right)$$

is lessening in each duration.

Based on the above results, a higher cooling rate at austenite transformation temperature should be taken in order to obtain small austenite grains. Thus, increasing the water flow in the mold to strengthen cooling intensity at about 1,400 ℃ is adopted to produce a fine austenite structure, which plays an important role in improving the ductility and eliminating transverse crack of slab at the straightening area.

4 Conclusions

(1) As temperature decreases, the amount of Ti and N dissolved in austenite gradually decrease, and partition coefficient x shows a gradually increasing tendency. The partition coefficient x is only about 0.04 when the temperature is between 1,350 ℃ and 1,440 ℃. The precipitation of Ti(C,N) has the characteristic "C" curve for diffusion and nucleation. Grain boundary nucleation is preferred for the nucleation location compared to homogeneous nucleation.

(2) Without considering the pinning effect on austenite growth, the model indicates the final size of austenite grain size would be 2.155 mm, 1.244 mm, 0.965 mm, 0.847 mm and 0.686 mm under the cooling rate of 1, 3, 5, 7, 10 ℃·s^{-1}. For the model considering the pinning effect, grain growth is found to remain stable from 1,350 ℃, and the final austenite grain size would

Table 5: Measured austenite sizes under different cooling rates

	Cooling rate (℃·s^{-1})				
	1	3	5	7	10
Grain size (mm)	1.41	1.08	0.78	0.61	0.48

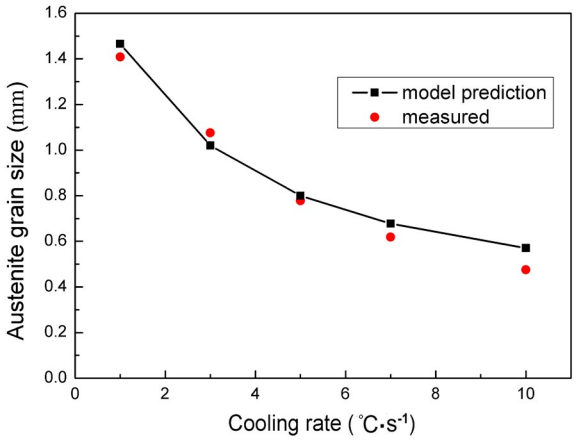

Fig. 11: Predicted sizes and measured sizes of austenite grains under different cooling rates

be only 1.46 mm, 1.02 mm, 0.80 mm, 0.67 mm and 0.57 mm. By determinant factors of the diffusion coefficient of titanium and solubility element (Ti, N) in the austenite grain boundaries, the final sizes of Ti(C_xN_{1-x}) precipitates are 137 nm, 79 nm, 61 nm, 51 nm and 43 nm, respectively, with an increase in the cooling rate from 1 to 10 ℃·s^{-1}.

(3) According to thermal tensile testing and OM observation on the micro-alloyed steel, the experiment results are consistent with calculation results in terms of austenite size. The corresponding countermeasure of increasing the water flow in the mold is proposed to improve the ductility and eliminate transverse crack of slab.

References

[1] Weng Yuqing. Ultrafine grained steel. Metallurgical Industry Press, 2003: 290–292. (In Chinese).
[2] Gunabalapandian K, Samanta S, Ranjan R, et al. Investigation of austenitization in low carbon micro-alloyed steel during continuous heating. Metallurgical & Materials Transactions A, 2017, 48(5): 2099–2104.
[3] Derda W, Wiedermann J. Some aspects of continuous casting of low carbon micro-alloyed steels with niobium and titanium. Archives of Metallurgy & Materials, 2012, 57(1): 303–310.
[4] Li Y, Chen X, Liu K, et al. Reasonable temperature schedules for cold or hot charging of continuously cast steel slabs. Metallurgical and Materials Transactions A, 2013, 44(12): 5354–5364.
[5] Dippenaar R, Bernhard C, Schider S, et al. Austenite grain growth and the surface quality of continuously cast steel. Metallurgical and Materials Transactions B, 2014, 45(2): 409–418.
[6] Li Y, Wen G, Luo L, et al. Study of austenite grain size of Micro-alloyed steel by simulating initial solidification during continuous casting. Ironmaking & Steelmaking, 2015, 42(1): 41–48.
[7] Dong D, Chen F, Cui Z. Modeling of austenite grain growth during austenitization in a low alloy steel. Journal of Materials Engineering and Performance, 2016, 25(1): 1–13.
[8] Lee S J, Lee Y K. Prediction of austenite grain growth during austenitization of low alloy steels. Materials & Design, 2008, 29(9): 1840–1844.
[9] Den Ouden D. Mathematical modelling of nucleating and growing precipitates: distributions and interfaces. Dissertation, Delft University of Technology, 2015.
[10] Perrard F, Deschamps A, Maugis P. Modelling the precipitation of NbC on dislocations in α-Fe. Acta Materialia, 2007, 55(4): 1255–1266.
[11] Xiao N, Tong M, Lan Y, et al. Coupled simulation of the influence of austenite deformation on the subsequent isothermal austenite–ferrite transformation. Acta Materialia, 2006, 54(5): 1265–1278.
[12] Miettinen J, Louhenkilpi S, Holappa L. Coupled simulation of heat transfer and phase transformation in continuous casting of steel. ISIJ International, 1996, 36(Suppl): S183–S186.
[13] Yasumoto K, Nagamichi T, Maehara Y, et al. Effects of alloying elements and cooling rate on austenite grain growth in solidification and the subsequent cooling processes of low alloy steels. Tetsu-to-Hagane, 1987, 73(14): 1738–1745.
[14] Bernhard C, Reiter J, Presslinger H. A model for predicting the austenite grain size at the surface of continuously-cast slabs. Metallurgical and Materials Transactions B, 2008, 39(6): 885–895.
[15] Wang Mingling, Yang Chunzheng, Tao Hongbiao. Formation mechanism of transverse corner crack on micro-alloyed steel slab. Iron and Steel, 2012, 47(10): 27–33 (In Chinese).
[16] Lei Jialiu, Xue Zhengliang, Jiang Yuedong, et al. Effect of carbon content on TiN inclusion precipitation in tire cord steel. Journal of Materials and Metallurgy, 2014, 13(2): 125–127 (In Chinese).
[17] Yong Qilong. Secondary Phases in Steels. Metallurgical Industry Press, 2006: 357–392 (In Chinese).
[18] Andersen I, Grong O. Analytical modelling of grain growth in metals and alloys in the presence of growing and dissolving precipitates. Normal Grain Growth. Acta Metallurgica et Materialia, 1995, 43(7): 2673–2688.
[19] Hu H, Rath B B. On the time exponent in isothermal grain growth. Metallurgical and Materials Transactions B, 1970, 1(11): 3181–3184.
[20] Uhm S, Moon J, Lee C, et al. Prediction model for the austenite grain size in the coarse grained heat affected zone of Fe-C-Mn steels: Considering the Effect of Initial Grain Size on Isothermal Growth Behavior. ISIJ International, 2004, 44(7): 1230–1237.
[21] Ma Fangjun. Precipitation behavior of the second phase and microstructural evolution of the surface layer of mirco-alloyed slabs in continuous casting. Dissertation, Chongqing University, 2010 (In Chinese).
[22] Zener C. Theory of growth of spherical precipitates from solid solution. Journal of Applied Physics, 1949, 20(10): 950–953.
[23] Stock J. NbC and TiN precipitation in continuously cast micro-alloyed steels. Dissertation, Colorado University, 2014.
[24] Reiter J, Bernhard C, Presslinger H. Austenite grain size in the continuous casting process: Metallographic methods and evaluation. Materials Characterization, 2008, 59(6): 737–746.

This work was financially supported by the National Natural Science Foundation of China (No. 51504172) and (No. 51474163), and China Postdoctoral Science Foundation (No. 2015M572212).